J. Phys. C: Solid State Phys. **20** (1987) 3533–3552. Printed in the UK

# A detailed investigation of the $E$–$J$ characteristic and the role of defect motion within the flux-line lattice for high-current-density, high-field superconducting compounds with particular reference to data on $Nb_3Sn$ throughout its entire field–temperature phase space

D P Hampshire† and H Jones
The Clarendon Laboratory, Parks Road, Oxford OX1 3PU, UK

Received 22 December 1986

**Abstract.** This paper analyses the role of defects within the flux-line lattice of high-current-density superconductors. A simple model demonstrates that above the normal density distribution in critical currents the $E$–$J$ characteristic is linear with a resistivity many orders of magnitude less than the bulk flux-flow resistivity. The universality of the three free parameters that describe the defect motion is explicitly demonstrated by considering data on $Nb_3Sn$ throughout its entire superconducting phase.

## 1. Introduction

This paper considers the $E$–$J$ characteristic of high-current-density, high-field superconducting compounds and alloys. A simple model is considered which is used to analyse the motion of defects within the flux-line lattice (FLL). It is this mechanism which is considered to be the most significant for the movement of flux above the critical current in all high-current-density materials. This analysis is used to derive the three-parameter fit the authors have successfully used to characterise a number of high-current-density materials (Hampshire and Jones 1986a) and that is of the form

$$E = \rho_I \int_{-\infty}^{J} f(J_i)(J - J_i)\,\mathrm{d}J_i \tag{1}$$

where

$$f(J_i) = \frac{1}{(2\pi)^{1/2}} \frac{\beta}{\bar{J}_c} \exp\left\{-\tfrac{1}{2}\left[\beta\left(\frac{J_i - \bar{J}_c}{J_c}\right)\right]^2\right\}. \tag{2}$$

$E$ is the electric field, $J$ the transport current density and we introduce $J_i$ as the local critical current in a region $i$. Also, $\rho_I$ is the interaction resistivity, $\beta$ is the synchronisation constant and $\bar{J}_c$ is the mean critical current density.

† Present address: Applied Superconductivity Centre, University of Wisconsin–Madison, Madison, WI 53706, USA.

0022-3719/87/233533 + 20 $02.50  

In the next section a brief summary of bulk flux flow in defect-free systems and in particular the nature of the flux-flow resistivity $\rho_f$ is addressed. In the third section these concepts are incorporated in a simple model used to describe defect motion in the FLL. In the fourth section this idealised model is generalised to consider highly pinned systems and an interpretation of the physical parameters $\beta_I$, $\beta$ and $J_c$ is given. The fifth section demonstrates the compatibility between the three-parameter fit (equation (1)) and the empirical two-parameter law, which is often used to characterise the structure of the $E$–$J$ characteristic (Walters 1974) of the form

$$E = \alpha J^n \tag{3}$$

where $\alpha$ (the alpha parameter) and $n$ (the index) are constants.

The functional form in field–temperature ($B$–$T$) space of the empirical parameters $\alpha$ and $n$ can thus be given a physical interpretation through the parameters $\rho_I$, $\beta$ and $J_c$. In the sixth section specific data that have been generated on $Nb_3Sn$ modified-jelly-roll (MJR) in the range $2.5\ \text{K} \leqslant T < T_c$, $1 \leqslant B \leqslant 15\ \text{T}$ are explicitly considered within the general framework given for flux flow in high-current-density materials, and the universality of the three parameters is demonstrated. This paper concludes by presenting the disconcerting reservations the authors have on the validity of the comparison between data from nominally defect-free systems and the theoretical understanding of the flux-flow resistivity.

## 2. Defect-free systems

There has been a great deal of theoretical and experimental work on the bulk motion of the FLL through defect-free systems. There are considered to be three main sources of energy-dissipation: the flow of a normal current within the moving core of a fluxon (Bardeen and Stephen 1965); the relaxation in the order parameter towards its equilibrium state when it is forced to vary in time as the flux flows (Tinkham 1964); and the slow-diffusion mechanism which is essentially a relaxation of the order parameter caused by the anomalous term in the microscopic theory (Gorkov and Kopnin 1973). The relative importance of these different contributions has been calculated at different field and temperature limits for different values of the Ginzburg–Landau parameter $K$. However, in all cases

$$E = \rho_f J \tag{4}$$

where $\rho_f$ is the flux-flow resistivity. More specifically, the theoretical analyses and experimental data suggest that

$$\lim_{B \to 0} \rho_f \propto B \qquad \text{for all } K.$$

Experimentally, it has not been possible to produce materials obeying equation 4. It is clear that even if the superconductor is perfectly stoichiometric and defect-free, the surfaces of the superconductor provide the possibility of flux-pinning. Thus in general it is found that

$$E = \rho(J - J_c) \tag{5}$$

where $\rho$ (the resistivity) and $J_c$ (the critical current) are independent of $E$ and $J$. It is then assumed that one can equate the resistivity in equation 5 with the flux-flow resistivity.

Assuming the validity of this identity demands that the mechanism for dissipation is unique, namely the bulk motion of the entire FLL. This will be discussed further in the concluding comments in this paper.

## 3. Flux flow in an idealised highly pinned composite

The first part of this section considers the properties of an idealised circuit which will be used as a framework to discuss the motion of defects in the FLL. The second part considers the experimental evidence for defect flow being the dominant mechanism for voltage generation above $I_c$.

### *3.1. A simple model for flux flow*

Consider an idealised superconducting path of unit area and unit length. This path consists of two regions A and B in series. Region A which occupies a fraction $F$ of the total length has a critical current $I_c'$, the rest of the path has a critical current $I_c''$ (where $I_c' < I_c''$). Although these two regions have different pinning-site configurations (and thus different critical currents) when bulk flux flow occurs it is assumed that they have the same characteristic flux-flow resistivity, $\rho_f$. Thus for each region, the $V$–$I$ characteristic is as follows. For region A:

$$V = 0 \qquad \text{for } I \leqslant I_c'$$

$$V = F\rho_f(I - I_c') \qquad \text{for } I \geqslant I_c'.$$

For region B:

$$V = 0 \qquad \text{for } I \leqslant I_c''$$

$$V = (1 - F)\rho_f(I - I_c'') \qquad \text{for } I \geqslant I_c''.$$

Thus the $V$–$I$ characteristic of the entire circuit is:

$$V = 0 \qquad \text{for } I \leqslant I_c' \tag{6}$$

$$V = F\rho_f(I - I_c') \qquad \text{for } I_c' \leqslant I \leqslant I_c'' \tag{7}$$

$$V = \rho_f\{I - [FI_c' + (1 - F)I_c'']\} \qquad \text{for } I \geqslant I_c''. \tag{8}$$

Thus the $V$–$I$ characteristic of this path consists of three linear regions (equations 6–8). At low transport current the path is truly superconducting. At high current, there is the bulk motion of all flux present which is characterised by the flux-flow resistivity. However there is also an intermediate current domain when only a small fraction of the total number of fluxons are moving, governed by equation 7, or equivalently:

$$V = \rho_I(I - I_c)$$

where $\rho_I$ (the interaction resistivity) $= F\rho_f$, and $I_c = FI_c' + (1 - F)I_c''$.

In this current path, some fluxons well below criticality are coupled with other fluxons at criticality. This crucial feature of two species of fluxons coupled together (i.e. experiencing the same transport current) leads to regions of very low resistance. There is an obvious analogy here with crystals where the presence of defects reduces their

critical stress by many orders of magnitudes. This coupling can occur in high-$K$ superconductors where, because there is much overlapping of fluxons, the transport current at any point interacts with many fluxons simultaneously.

Hence it can be seen that this simple model can be used to consider the motion of defects in the FLL in superconducting systems.

Below $I_c'$ there is no flux motion and the system can be said to be truly superconducting. At $I_c'$ all the defects in the FLL are at criticality. Above $I_c'$ the defects in the FLL flow across the superconductor (in much the same way that defects flow across crystals above their critical stress). This leads to a resistivity many orders of magnitude less than the bulk flux-flow resistivity. This is just the result that has been found by the authors for the high-current-density materials NbTi, $V_3Ga$ and $Nb_3Sn$—typically $\rho_I < 10^{-5}\rho_f$.

It is clear that this model does not consider many of the complexities of defect motion such as: defect–defect interactions; different types of defects; and defect production. However despite avoiding the complexities associated with considering all the different types of defects in the FLL, the main theme of the model describing defect motion remains. The general $E$–$J$ characteristic is given by

$$E = \rho_I(J - J_c) \tag{9}$$

where $J_c$ is the maximum critical current for which there is no flux motion, and $\rho_I$, the interaction resistivity, is many orders of magnitude less than the flux-flow resistivity characteristic of bulk flux flow.

### *3.2. Experimental evidence for defect motion in the FLL*

Four sources of experimental evidence that suggest the importance of defect motion in the FLL are considered below.

(i) *Noise measurements.* Measurement of the noise emitted from superconductors during flux flow demands that fluxon bundles do not simply traverse the width of the superconductor in one continuous movement. Rather, flux bundles experience intermittent periods of motion and periods of being static (Habbal and Joiner 1977). This is consistent with the model of defect motion considered.

(ii) *The history effect.* It has been demonstrated that the critical current at a given field and temperature is dependent on the path in phase-space by which the field and temperature is achieved (Kupfer and Meier-Hirmer 1985). It is clear that the number and type of dislocations in the FLL is determined by the interaction between the FLL and the underlying microstructure. Since the FLL can achieve many possible disordered configurations we do not expect a unique number and type of defect at a given field and temperature. Thus it is clear that the model presented is consistent with the critical current not being a unique function of field and temperature.

(iii) *Direct observation of defects in the FLL.* Using decorative techniques (Essmann and Trauble 1967) and SEM (Singh *et al* 1976), direct observation of defects in the FLL have been observed.

(iv) *The interaction resistivity.* The data on $Nb_3Sn$ presented in this paper will demonstrate that the effective resistivity above the normal distribution in $I_c$ is seven orders of magnitude lower than that expected were all fluxons to be in motion. This is consistent with the generation of voltage above $I_c$ being due to the motion of defects and thus only a small fraction of the fluxons being in motion at any given time.

## 4. Flux flow in highly pinned, inhomogeneous superconducting compounds

Even a preliminary investigation of the microstructure of high-current-density materials suggests significant variation of the pinning strengths and thus the critical current along the length of the composites. A superconducting composite can be considered to consist of a large number of component regions each with its own characteristic critical current. The total electric field generated is now a superposition of those of the type given by equation 9 as was suggested by Jones and co-workers (1967). Thus, this can be generalised to give an $E$–$J$ characteristic of the form

$$E = \sum_{i \text{ for } J_i < J} \rho_i (J - J_i)$$

or for a large number of component regions

$$E = \int_{-\infty}^{J} \rho_i f(J_i)(J - J_i)\, \mathrm{d}J_i \tag{10}$$

where $f(J_i)$ characterises the distribution in the critical currents for the component regions.

Baixeras and Fournet (1967) have used equation 10 to characterise high-current-density materials. Their interpretation of $f(J_i)$ was such as to consider a unique value for $J_c$ beyond which moving fluxons interacted with stationary fluxons causing them to move. The derivation given here does not require the introduction of an interaction of this sort but rather only a distribution in the critical currents of the component regions.

In the analysis of the data on MJR $Nb_3Sn$ it is assumed that $f(J_i)$ is the normal density function given by equation 2. The primary justification for this assumption is that it describes our data presented previously on NbTi (Hampshire and Jones 1986a) and the data presented here on $Nb_3Sn$. Evetts and Plummer (1985) have pointed out that since the different sources of inhomogeneity that determine $J_c$ are independent the central-limit theorem demands that $f(J_i)$ is likely to be very close to a normal density function. Recently the essentially 'bell-shaped' form of the distribution has been confirmed by Warnes and Larbalestier (1986) using direct deconvolution by using the equation (Jones *et al* 1967)

$$\partial^2 E / \partial J^2 = \rho_f f(J). \tag{11}$$

However, in the range of currents considered, it will be demonstrated that $\rho_f$ in equation 11 should be replaced by $\rho_I$.

The interpretation of the three free parameters in the $E$–$J$ characteristic are now considered in turn.

### *4.1. The interaction resistivity, $\rho_I$*

It is clear from the model outlined above that the interaction resistivity is determined by the number and type of defects in the FLL that are present—characterising the resistivity of the superconductor when all the defects in the FLL are in motion. It is not strictly a unique function of field/temperature but has been found to be as such, to within experimental error. Its functional form is determined essentially by the interaction between two structures—the underlying pinning structure and the FLL. It is assumed in

the analysis below that it is uniquely determined by the average thermodynamic properties of the superconductor and is thus independent of the local critical current. Its size is many orders of magnitude less than the flux-flow resistivity.

### *4.2. The synchronisation constant, $\beta$*

Any elementary statistics text gives the result that the standard deviation $\sigma$ of the distribution in the current density is

$$\sigma = \bar{J}_c/\beta = [(J_i)^2 - (\bar{J}_c)^2]^{1/2} \Rightarrow 1/\beta^2 = [\overline{J_i^2} - (\bar{J}_c)^2]/(\bar{J}_c)^2. \tag{12}$$

It can be seen from equation 12 that the size of $\beta$ gives a measure of the width of the distribution of critical currents and the $B$–$T$ dependence of $\beta$ gives the different $B$–$T$ dependences that operate in the component regions of the composite.

Consider a particular point in $B$–$T$ space at which for two different component critical currents $J'$ and $J''$, they are such that $J' > J''$. Then assuming the most simple case, namely that this inequality holds throughout the entire superconducting phase for *all* $J''$, $J'$, then in general we have

$$f(J')/f(J'') = p_i$$

where $p_i$ is independent of both field and temperature, and $f$ is defined in equation 2.

If we let $J'' = J_c$

$$\exp\left\{-\tfrac{1}{2}\left[\beta\left(\frac{J' - \bar{J}_c}{\bar{J}_c}\right)\right]^2\right\} = p_i \Rightarrow J' = \bar{J}_c\left(1 \pm \frac{(2\ln(1/p_i))^{1/2}}{\beta(B, T)}\right). \tag{13}$$

It is clear that equation 13 is the general equation giving the $B$–$T$ dependence of an arbitrary component of the distribution in critical currents. The identity of this component is defined by the constant $p_i$.

The three most significant cases for the functional form of $\beta(B, T)$ are now briefly discussed.

(i) $\beta(B, T) =$ constant

In this case for all $p_i$:

$$J' = C\bar{J}_c(B, T).$$

Thus all the component regions of the composite obey an identical scaling law differing only by a constant prefactor $C$.

(ii) $\beta(B, T) = \beta(b)$ (or similarly $\beta(B, T) = \beta(T)$)

If we consider the mean critical current to obey a Fietz–Webb scaling law of the form

$$\bar{J}_c(B, T) = C^* H_{c2}^n(T) f(b)$$

where $C^*$ is a constant and $b = B/B_{c2}(T)$, then

$$J'(B, T) = C^* H_{c2}^n(T)\{[1 + (2\ln(1/p_i))^{1/2}/\beta(b)]f(b)\}.$$

Thus all the component critical currents have an identical temperature dependence but have different reduced-field dependences depending on the value for $p_i$ (or equivalently which particular region is considered). This case is found over a limited range for the MJR $Nb_3Sn$ data considered below.

(iii) $\beta(B, T) = \beta(b, T)$

In this case if the critical-current distribution function is *strictly* a normal density function for all fields and temperatures, it is clear that even if $J_c(B, T)$ obeys a Fietz–Webb scaling law, the functional form of the critical current for all other component regions cannot be expressed in terms of a scaling law.

However if we relax the condition that the distribution function for the critical currents is rigorously a normal density function, and assume that it is in fact a good approximation to a generalised bell-shaped distribution, then $\beta(B, T)$ is essentially the parameter which delineates the 'tails' of the distribution from the central region.

From equation 13, in the 'tails' of the distribution ($p_i \rightarrow 0$), we have

$$J' = \pm C^* H_{c2}^n(T) f(b) \left( \frac{1}{\beta(b, T)} (2 \ln(1/p_i))^{1/2} \right).$$

It is clear that if $J'$ obeys a scaling law (i.e. $J' = CH_{c2}^m(T) f'(b)$) then

$$\beta(b, T) = \frac{C^* H_{c2}^n(T) f(b)}{C H_{c2}^m(T) f'(b)}.$$

Hence in the case that the component regions of the superconductor obey Fietz–Webb-type scaling laws of different field and temperature dependences, then the normal distribution will best fit to this with $\beta$ obeying a universal scaling law.

This universality of $\beta$ has been observed by the authors for all high-current-density materials to date.

### *4.3. The mean critical current density, $J_c$*

This parameter is self-explanatory, being the mean value of the distribution of component critical currents.

## 5. The empirical formalism for the *E–J* characteristic

The *E–J* characteristic is often described by the empirical equation 3. It has been demonstrated by Plummer and Evetts (1986) that in the tails of the normal density function there is good agreement over many decades of voltage. By equating equations 1 and 3 and their first derivatives we find

$$n = (\pi/2)^{1/2} \beta \qquad \text{for } J \simeq \bar{J}_c \tag{14}$$

or equivalently

$$\sigma = \bar{J}_c/\beta = (\bar{J}_c/n)(\pi/2)^{1/2}$$

and

$$\rho_I = 2nE_{J=\bar{J}_c}(J)/\bar{J}_c = 2n\alpha \bar{J}_c^{n-1}. \tag{15}$$

Equations 14 and 15 give the empirical constants $\alpha$ and $n$ in terms of the physical parameters $\rho_I$, $\beta$ and $J_c$. Thus we can now give a physical interpretation for the field and temperature dependence of $\alpha$ and $n$. A specific case of this interpretation will be given when the data on the $Nb_3Sn$ MJR is considered.

## 6. The structure of the *E–J* characteristic for $Nb_3Sn$ MJR as a function of field and temperature throughout the superconducting phase

This section presents data on a $Nb_3Sn$ MJR composite which determines the empirical constants $\alpha$ and $n$ and the physical parameters $\rho_I$, $\beta$ and $J_c$ throughout the superconducting phase in the range $2.5\ K \leqslant T < T_c$ and $1 < B < 15\ T$.

In the first two parts brief descriptions of the particular composite used and the apparatus and techniques employed in deriving the data are given. In the third part the details of the two-parameter and three-parameter computerised fits are outlined. In the fourth part the critical current is presented as a function of field and temperature. In the fifth part the validity of the Fietz–Webb scaling law is demonstrated and the functional form of the pinning force explicitly derived. The sixth and seventh part demonstrate the universality of the interaction resistivity and the synchronisation constant. A comparison between these parameters using both equations 14 and 15 with their values derived directly from the three-parameter fit is detailed. The *B–T* dependence of the different Fietz–Webb laws that operate in the component parts of the composite are discussed.

### *6.1. A highly homogeneous high-current-density $Nb_3Sn$ MJR composite*

The details of the design of this jelly-roll wire composite have been detailed by Smathers *et al* (1984). In these modified configurations, the conventional central tin core is replaced by a copper core. Juxtapositioned around the core are two meshes of niobium and bronze (Cu 13.5 wt% Sn). Beyond the niobium/bronze layer is an outer sheath of copper. Tantalum diffusion barriers prevent the poisoning of the copper by tin during reaction. The critical feature of these composites is that during reaction each niobium filament sees an identical tin supply. Using TEM and Auger it has been demonstrated that these idealised MJR conductors are probably amongst the most uniform $Nb_3Sn$ high-current-density composites yet made.

The wire was reacted under vacuum ($<10^{-6}$ Torr) at 700 °C (±2 °C) for 170 h followed by 750 °C for 340 h. This reaction ensured the complete conversion of niobium to $Nb_3Sn$.

### *6.2. Measurements of the E–J characteristic*

The details of the apparatus and techniques employed have been described by Hampshire and Jones (1987). However a general outline is as follows.

At each fixed field and temperature a direct current was slowly increased through the helically wound superconducting specimen. Potential taps were positioned across 0.33 m of the sample which lay in a uniform magnetic field. Temperature control was maintained in two different modes: (i) $T < 4.2$ K. In this mode the sample lay in intimate thermal contact with the helium bath. The temperature was maintained using standard vapour pressure control (ii) $T > 4.2$ K. In this mode the sample was isolated from the helium bath but was in good thermal contact with a copper block which incorporates both heaters and thermometry. Feedback control between these elements ensures that during transport current flow the temperature of the sample remains constant throughout the measurement.

A hard-copy trace of the voltage as a function of current is obtained at each field and temperature using an *X–Y* recorder.

### *6.3. The two-parameter and three-parameter computerised fits*

The hard-copy $E$–$I$ characteristics were digitised between 10 and 90 $\mu V\ m^{-1}$ at 5 $\mu V\ m^{-1}$ intervals. Above $B_{c2}(T)$ the resistance of the sample (matrix) and sample holder was determined between the potential taps (the contribution of the superconductor in the normal state is negligible). This resistance was verified as being field and temperature independent above $B_{c2}(T)$ as expected in this cryogenic range by taking measurements at various temperatures. At each digitised $E$–$I$ data point, the current being shunted through this parallel Ohmic path was subtracted and the corrected current through the superconductor alone obtained as a function of voltage. Two points are worth mentioning.

(i) The uncertainty in temperature.

The uncertainty in temperature quoted is due to the temperature gradients that exist between the thermometers and the sample in our experimental apparatus. This has been

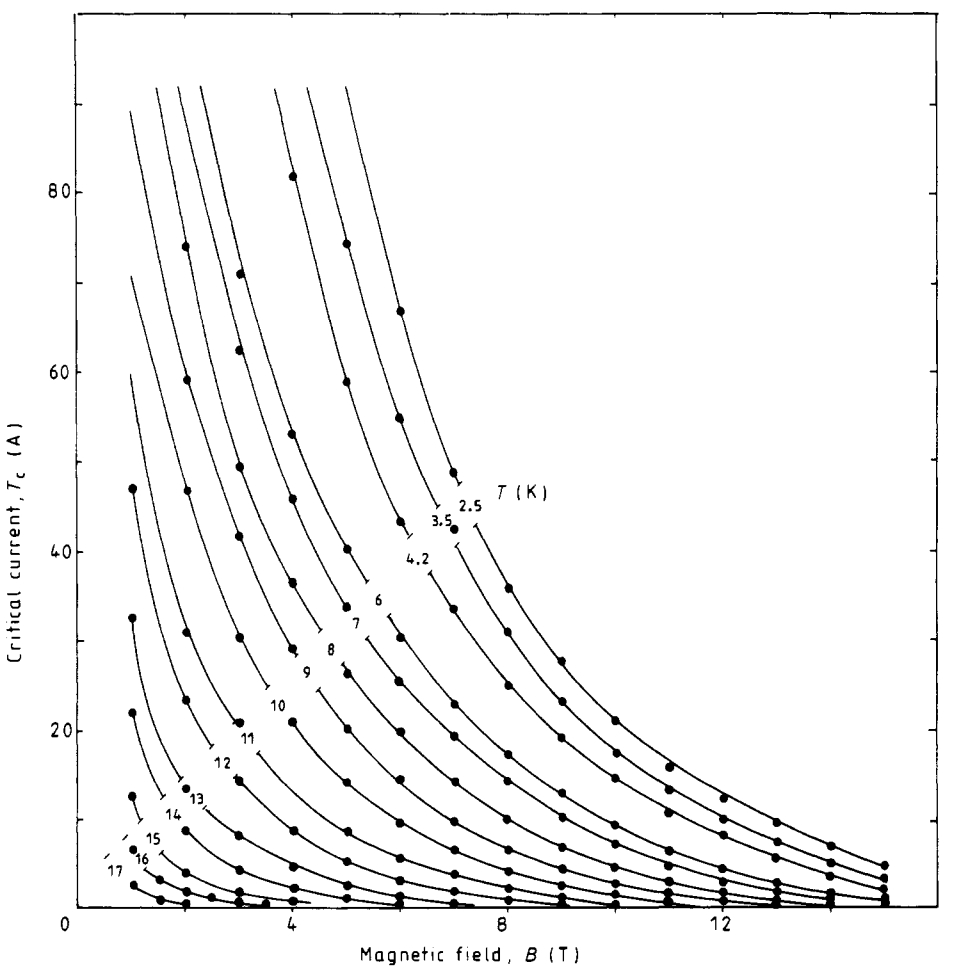


**Figure 1.** The critical current for MJR $Nb_3Sn$ as a function of field and temperature.

considered in detail and was shown to be $\pm 0.05$ K for $T \leqslant 4.2$ K and $\pm 0.025$ K for $4.2\text{ K} < T < T_c$.

(ii) Non-reversibility of the $E$–$I$ transition.

This is always expected to some degree since critical current is not a fundmental thermodynamic function. Experimentally the primary sources of non-reversibility are: instability in temperature control during the transition; non-zero time constants in electronic circuity; and electronic and thermal noise.

Non-reversibility causes an uncertainty in the voltage at any given current of typically $\pm 2\ \mu\text{V m}^{-1}$.

For the two-parameter fits, the corrected $E$–$I$ data were used in a least-squares program which determined $\alpha$ and $n$.

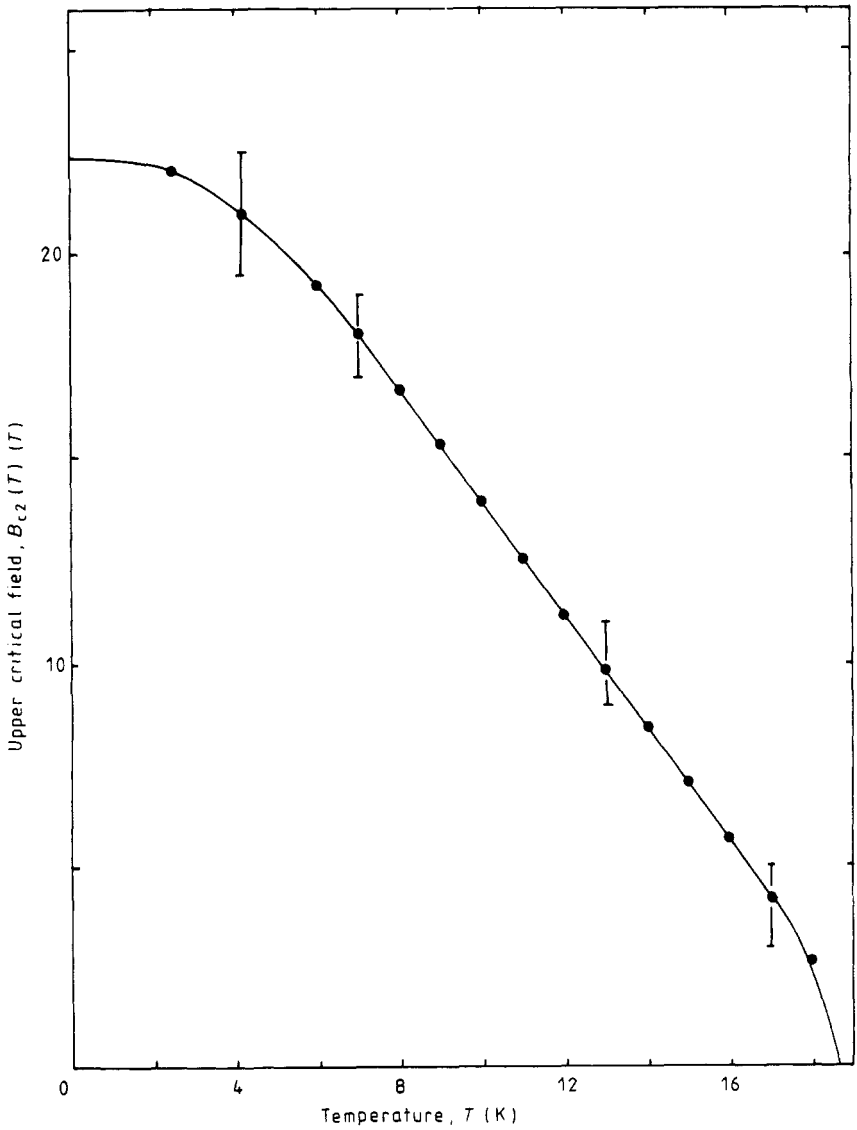


**Figure 2.** The upper critical field for MJR $Nb_3Sn$ as a function of temperature.

For the three-parameter fits, a direct determination of $\rho_I$, $I_c$ and $\beta$ was initially made using a non-linear least-square program. A smooth set of curves was then drawn through $\rho_I$, $I_c$ and $\beta$. In order to break any correlation between these three parameters, two-parameter fits were then completed by holding one of the parameters fixed at this value on the smooth curve and using the data to determine the other two parameters. This iteration process does not change the initial smooth set of curves determined. However these solutions have a standard deviation about the smooth curves reduced by about 30%. This additional iteration can be seen to determine values for the three parameters which are no longer those with the smallest 'sum of squares' but are physical values (obeying smooth functional forms) which are compatible with the uncertainty in electric field of typically $\pm 2\ \mu V\ m^{-1}$.

### 6.4. *The critical current as a function of field and temperature*

In figure 1, the critical current is presented as a function of field and temperature for $2.5\ K \leqslant T < T_c$ and $1 < B \leqslant 15\ T$. The difference between this current defined at an arbitrary voltage of $50\ \mu V\ m^{-1}$ and that obtained from the mean value of the distribution,

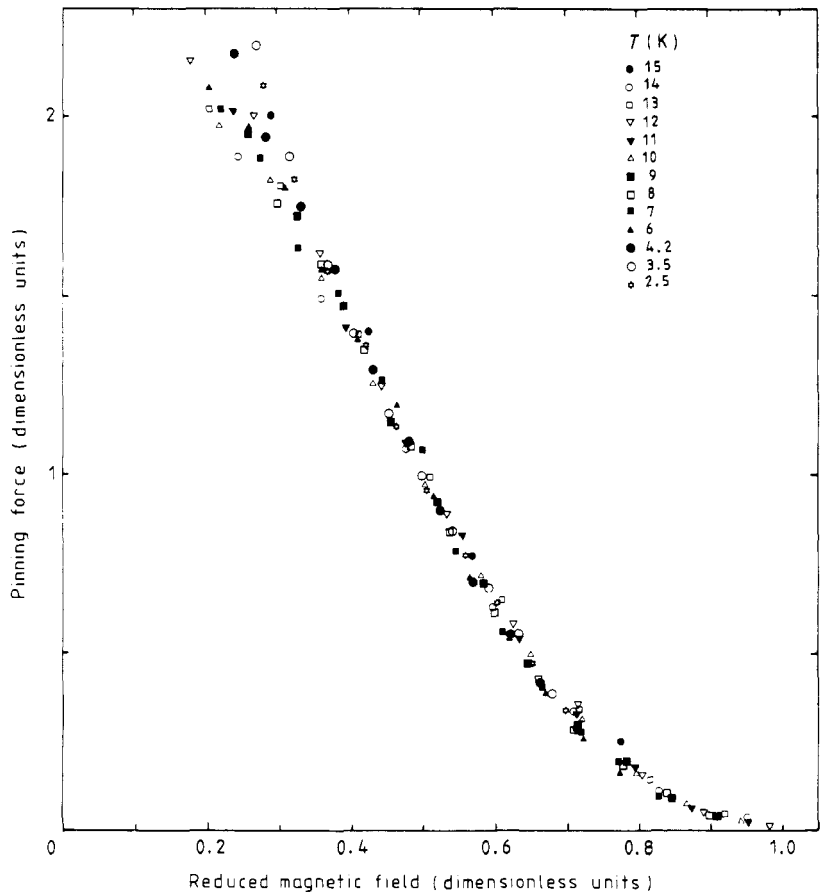


**Figure 3.** A universal curve—the normalised pinning force, $F_p(B, T)/F_p(B_{c2}(T)/2, T)$, plotted against the reduced magnetic field, $B/B_{c2}(T)$, for MJR $Nb_3Sn$.

$I_c$, is less than 1 A. To within the accuracy of these data there is no evidence for significant systematic variations throughout superconducting phase space for the electric field at which the mean critical current occurs. It will be shown below that the average electric field at which the mean critical current occurs is 55.3 $\mu$V m$^{-1}$.

### *6.5. The Fietz–Webb scaling law*

In figure 2 the upper critical field as a function of temperature is presented. This parameter has been determined by a smooth extrapolation of the critical current data to zero current. From this figure, two important critical parameters can be determined

$$B_{c2}(0) = 22.4 \pm 1.5 \text{ T}$$

$$T_c = 18.2 \pm 0.5 \text{ K}.$$

These values are very similar to the values found for pure, highly stoichiometric $Nb_3Sn$ (Foner and McNiff 1981).

In general the Fietz–Webb scaling law is tested by normalising the pinning force to unity at its maximum and then plotting the reduced pinning force versus the reduced magnetic field at different temperatures (Fietz and Webb 1969). However for this particular material there is no peak in the pinning force over the range of field and temperature considered—thus this technique cannot be used. An alternative technique is to normalise the pinning force at a fixed value of reduced magnetic field. An arbitrary value of $b$ $(=B/B_{c2}(t))$ of $\frac{1}{2}$ has been chosen although the results are essentially independent of the value chosen. The universal curve showing the normalised pinning force versus the reduced magnetic field is shown in figure 3. It is clear these data agree very well with a Fietz–Webb scaling law of the form

$$F_p = \alpha H_{c2}^n(T)[2.82 - 3.64b] \qquad \text{for } 0.2 \leqslant b \leqslant 0.7$$

where $\alpha = 11.2 \text{ N mm}^{-1} \text{ T}^{-3.12}$ if $F_p$ is the length pinning force, or $\alpha = 1.26 \text{ N mm}^{-3} \text{ T}^{-3.12}$ if $F_p$ is the volume pinning force, and $n = 3.12$.

The high-field concave tail in figure 3 is not explicitly considered in this work but is generally attributed to a distribution in $B_{c2}$ (Flukiger 1984).

### *6.6. The synchronisation constant $\beta$/index $n$*

This part presents the empirical index $n$ and the physical parameter $\beta$ throughout the superconducting phase. An interpretation of their functional form is discussed.

In figure 4 the index $n$ is presented as a function of field and temperature. There are two features of note: (i) the index decreases as the magnetic field increases; and (ii) at low temperatures the index is far less sensitive to temperature changes than at high temperatures.

In order to demonstrate the universality of the synchronisation constant, the values obtained at each temperature have been normalised to unity at $B_{c2}(T)/2$. Thus in figure 5 the reduced synchronisation constant as a function of reduced magnetic field presents the universal curve that characterise these data. In figure 6 the synchronisation constant at $B_{c2}(T)/2$ as a function of temperature is plotted. It can be seen that $\beta$ is only a function of reduced field for $T \leqslant 10$ K beyond which it decreases as the temperature increases. From the discusion of $\beta$ above, the universality of $\beta$ suggests that the component regions

of this composite obey different scaling laws of the Fietz–Webb type, where

$$\beta(b, T) = f_i(T)g_i(b)$$

for all the component regions $i$ of the composite.

It is concluded that for $T \leqslant 10$ K all the component regions have the same temperature dependence as the mean critical current (i.e. $f_i(T) = f(T)$). For $T \geqslant 10$ K, the decrease in $\beta(B_{c2}(T)/2, T)$ at higher temperatures implies that higher critical currents decrease less than lower critical currents as the temperature increases. The trend in figure 5 can be interpreted as showing that as the reduced field increases the critical currents in the low-current tail of the distribution decrease by more than the critical currents in the high-current tail.

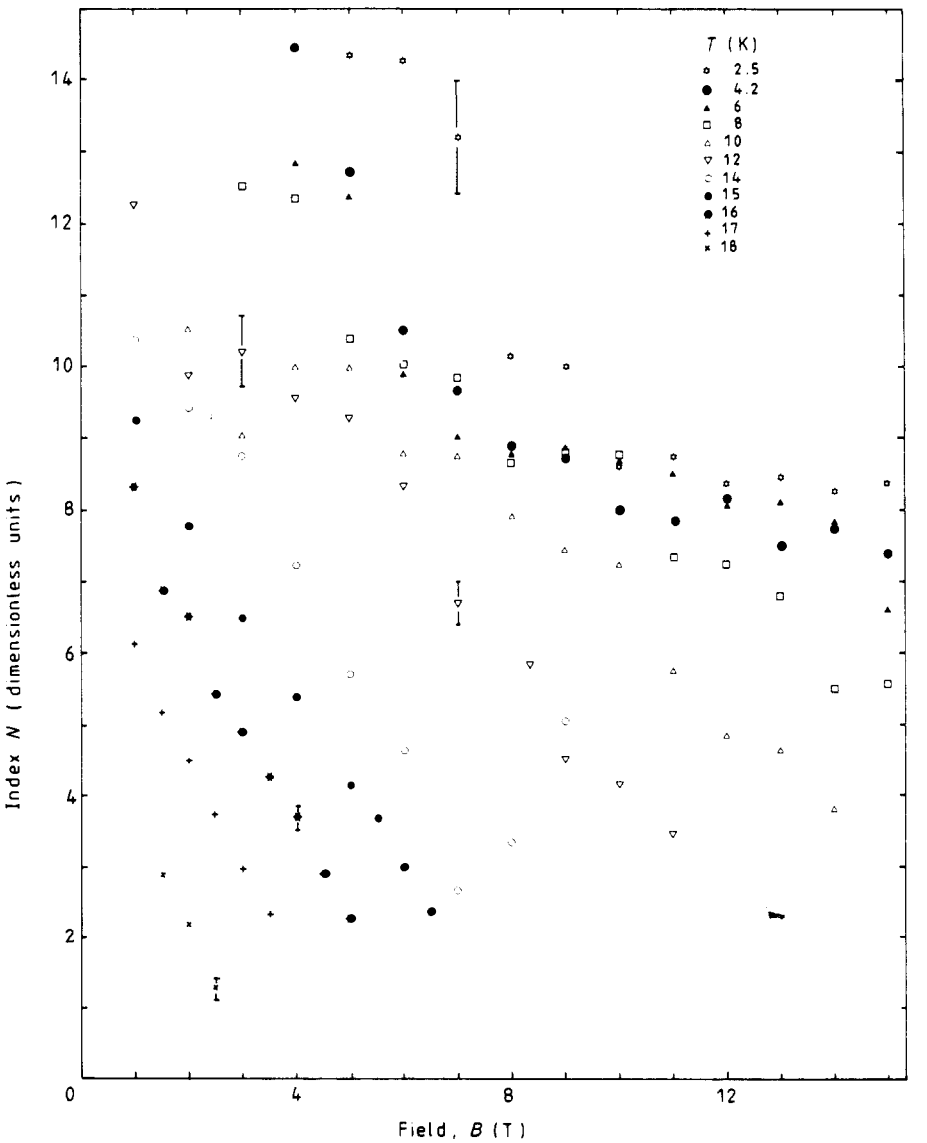


**Figure 4.** The index $n$ as a function of field and temperature for MJR $Nb_3Sn$.

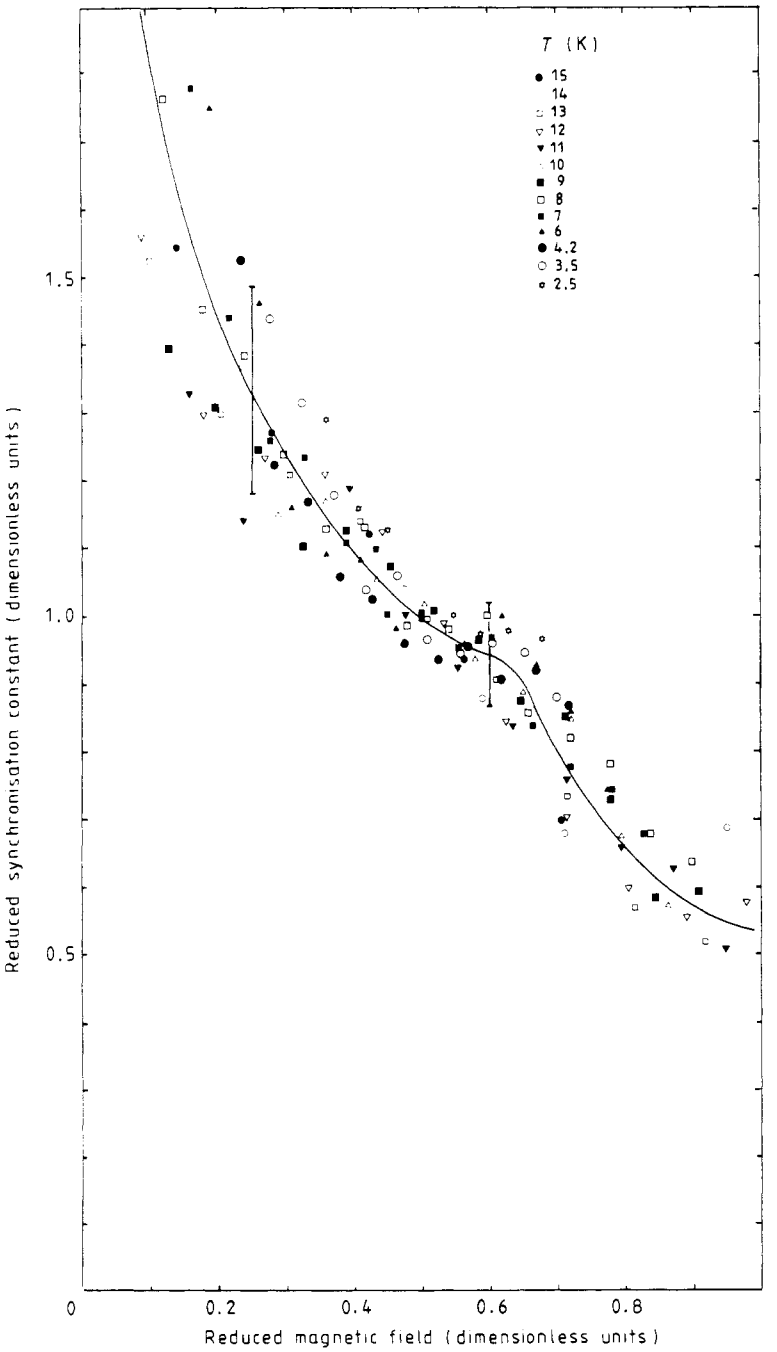


**Figure 5.** The reduced synchronisation constant, $\beta(B, T)/\beta(B_{c2}(T)/2, T)$, as a function of reduced magnetic field, $B/B_{c2}(T)$, for MJR $Nb_3Sn$.

The error bars shown in figures 5 and 6 are characteristic of fluctuations in the temperature during the transition of about 0.1 K. However we expect the variation in temperature to be significantly less than this. The scatter that is seen is attributed to the normal distribution being only an approximation to the bell-shaped distribution that rigorously characterises this material. To within the error of the data considered in this section, in agreement with equation 14, it is clear that $\beta$ and $n$ have the same characteristics throughout the superconducting phase.

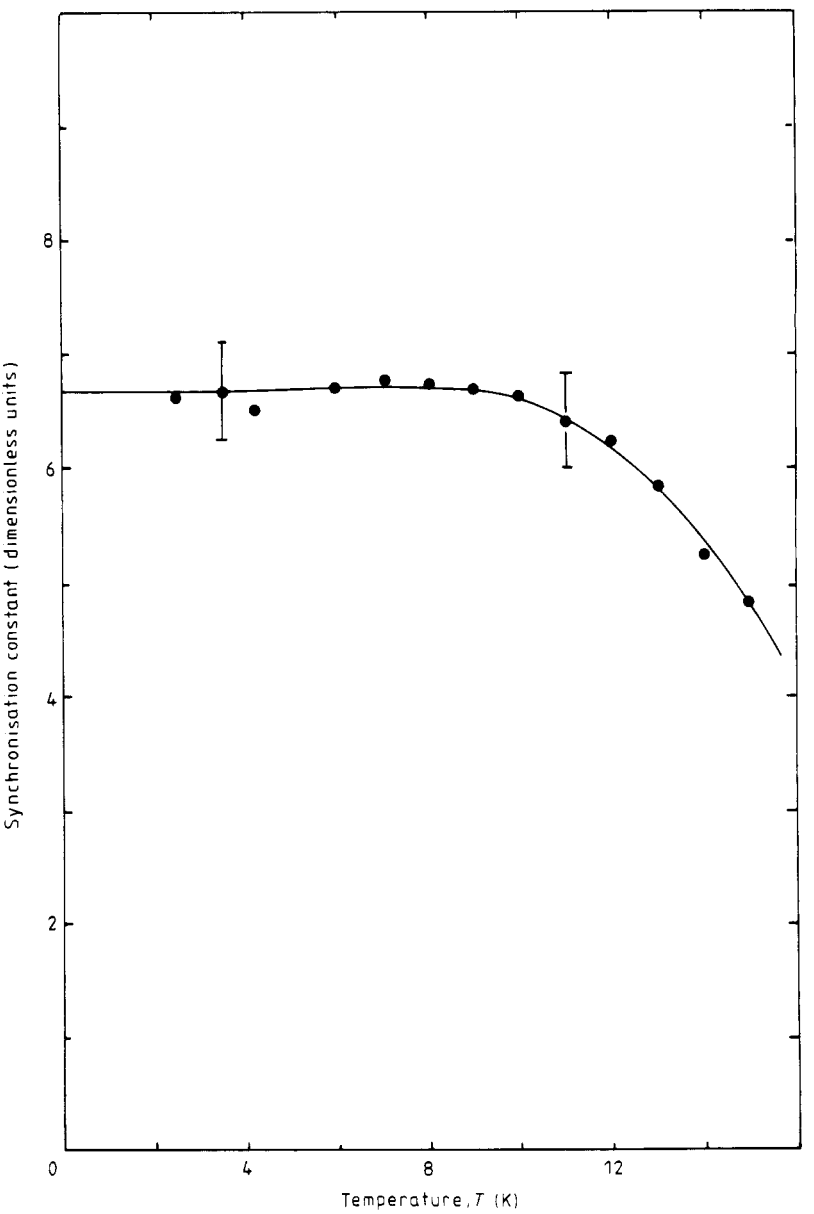


**Figure 6.** The synchronisation constant, $\beta(B_{c2}(T)/2, T)$ as a function of temperature for MJR $Nb_3Sn$.

*6.7. The universality of the interaction resistivity*

From the data given in figures 1 and 4, the empirical interaction length resistance $R_{IL}$ can be determined at each field–temperature point by using

$$R_{IL}(B, T) = 2nE_{I=\bar{I}_c}(I)/\bar{I}_c$$

where $E = 50\ \mu V\ m^{-1}$ and $I_c$ is the current at $50\ \mu V\ m^{-1}$. This parameter is plotted in figure 7 as a function of field and temperature every 2 K (the interaction-length resistance

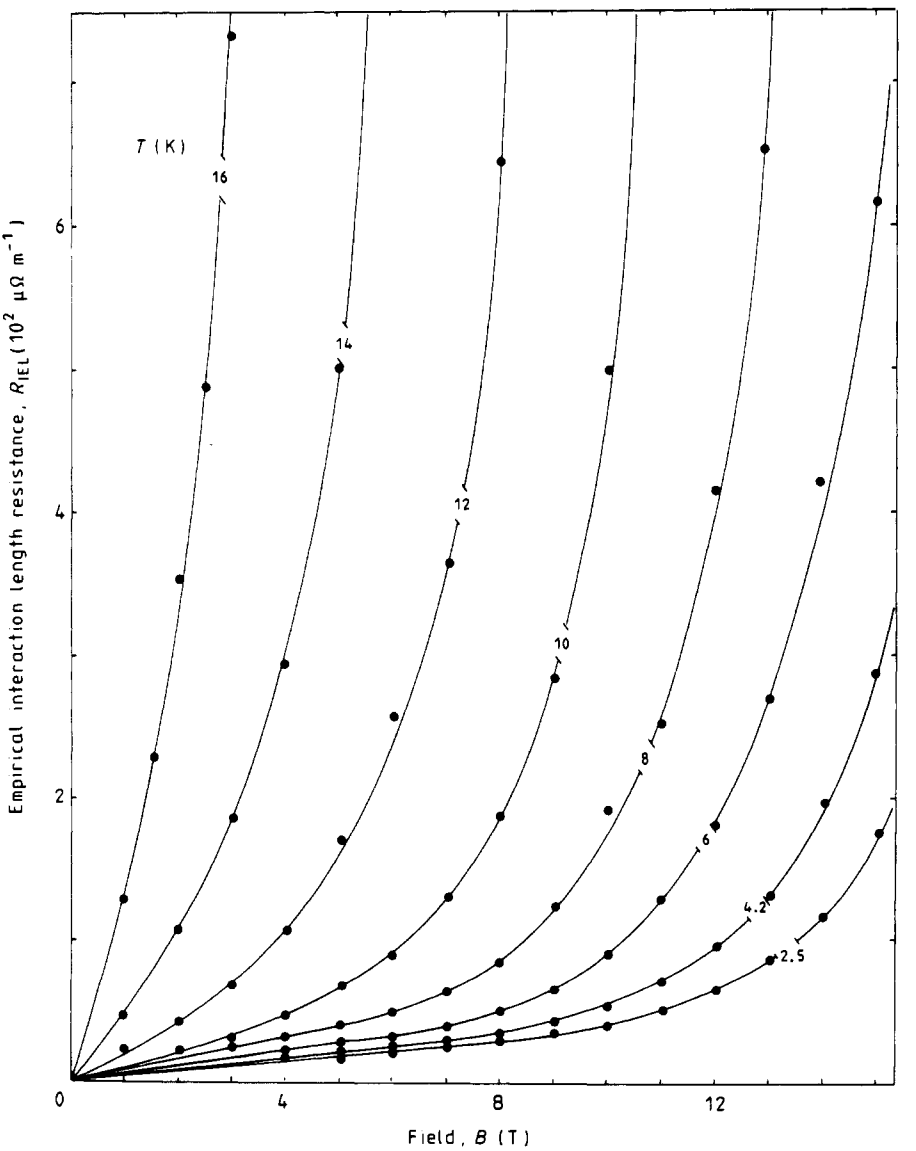


**Figure 7.** The empirical interaction-length resistance as a function of field and temperature for MJR $Nb_3Sn$.

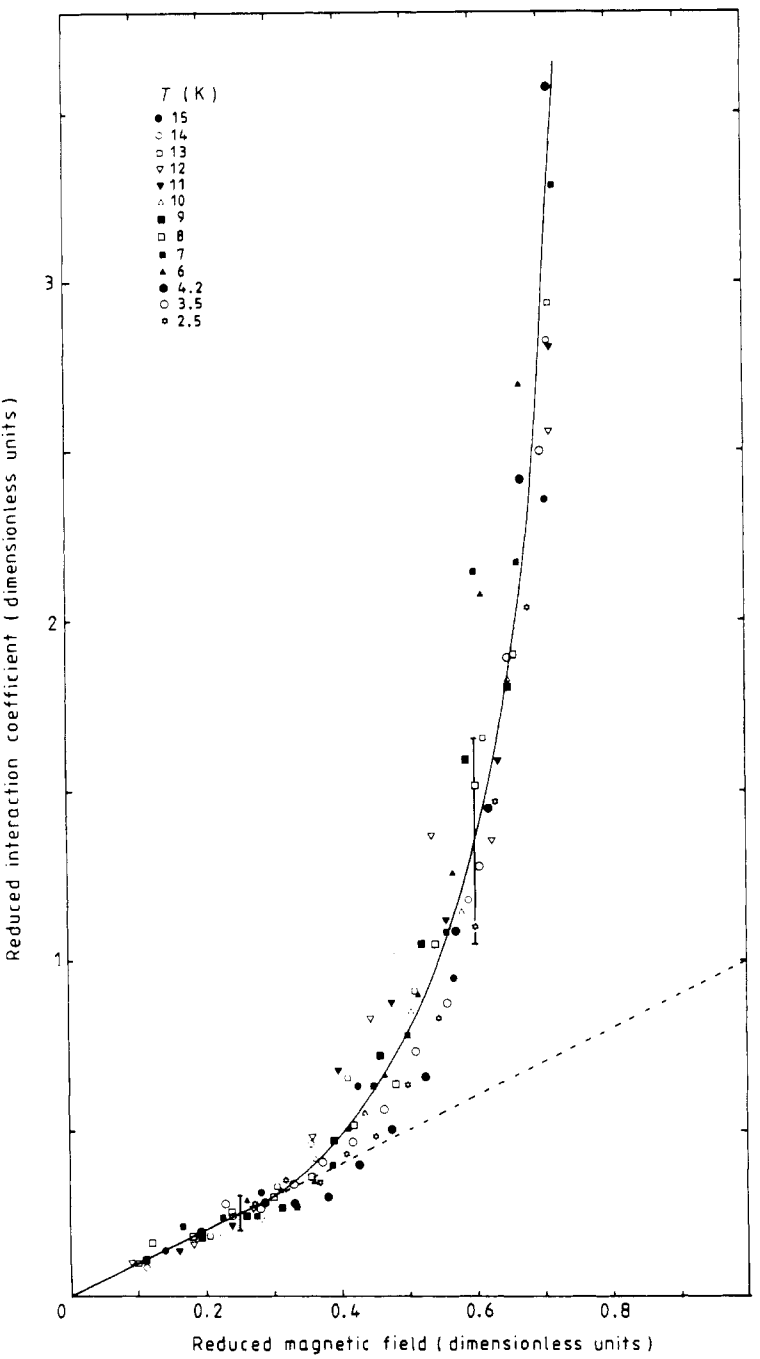


**Figure 8.** The reduced interaction coefficient, $\alpha^*$, as a function of reduced magnetic field, $B/B_{c2}(T)$.

can be converted to an interaction resistivity using a value of $8.8 \times 10^{-2}$ mm$^2$ for the area of $Nb_3Sn$.) A universal law of the form

$$R_{IL}(b, T) = R_I(0)bK(b)L(T/T_c)$$

where $\lim_{b\to 0} K(b) = 1$, $\lim_{r\to 0} L(T/T_c) = 1$ and $R_I(0)$ is a constant, can be used to characterise these data.

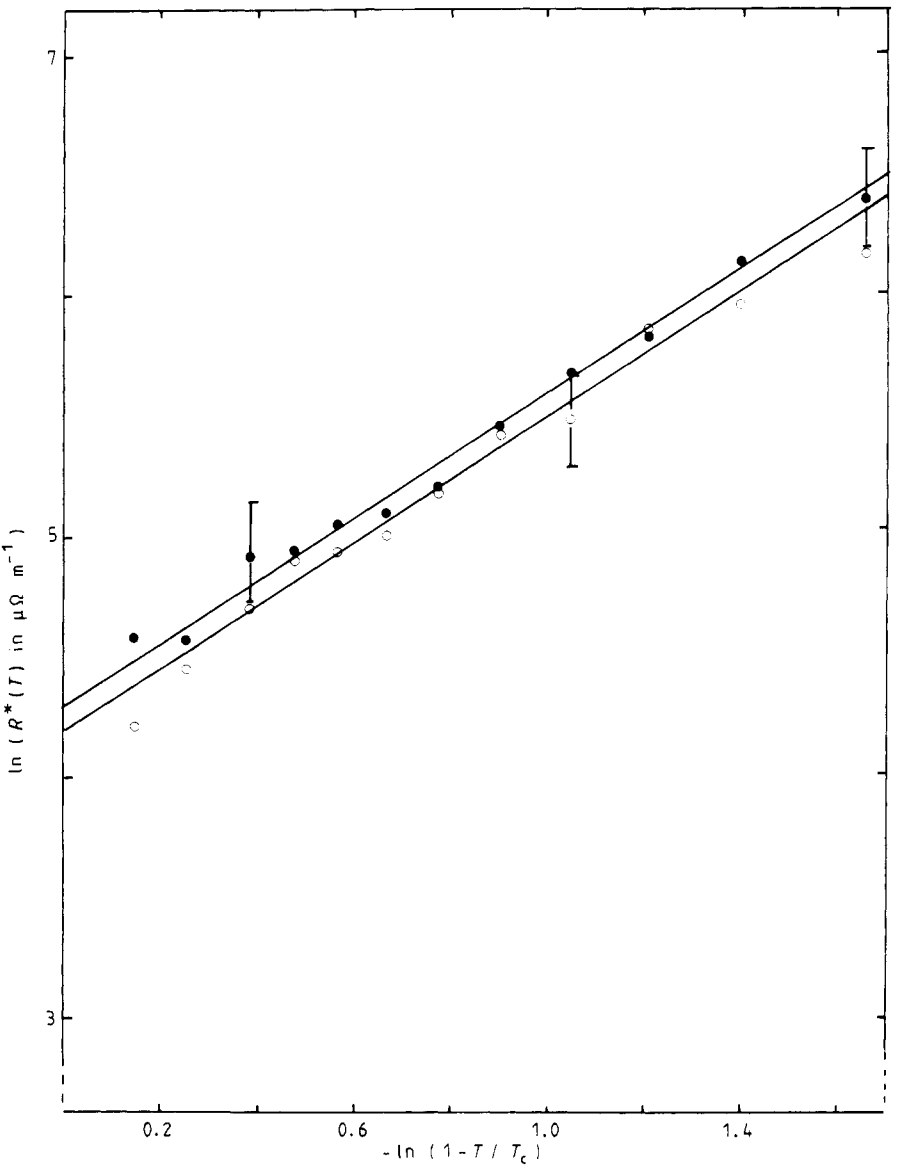


**Figure 9.** A plot of $\ln(R^*(T))$ against $-\ln[1 - (T/T_c)]$.

$$\left(R^*(T) = \lim_{B\to 0} \frac{\partial R_{IL}(b, T)}{\partial B} B_{c2}(T)\right)$$

Full circles represent values calculated from a three-parameter fit and open circles those derived at 50 $\mu$V m$^{-1}$ from the empirical two-parameter law.

In figure 8, the reduced interaction coefficient $\alpha^*$ is plotted as a function of magnetic field, where

$$\alpha^* = R_{IL}(B, T)/R^*(T)$$

and the normalisation constant $R^*(T)$ is

$$R^*(T) = \lim_{B\to 0}\left(\frac{\partial R_{IL}(B, T)}{\partial B} B_{c2}(T)\right) = R_I(0)L\left(\frac{T}{T_c}\right).$$

In figure 9, $\ln(R^*(T))$ is plotted against $\ln(1 - T/T_c)$ where $R^*$ is determined both from the empirical two-parameter law and the three-parameter fit. Thus we can conclude

$$R_{IL}(B, T) = R_I(0)bK(b)/[1 - (T/T_c]^n.$$

where $n = \frac{4}{3} \pm \frac{1}{3}$ and $R_{IL}(0) = 63.5\ \mu\Omega\ m^{-1}$ (or equivalently for the $Nb_3Sn$ alone $\rho_I(0) = 5.63 \times 10^{-4}\ \mu\Omega$ cm) for the full three-parameter fit.

That the two lines are parallel in figure 9 is a manifestation of the constancy of the electric field at which the mean critical current occurs. It is clear that were the empirical parameters determined assuming that the mean critical current occurred at $55.3\ \mu V\ m^{-1}$, equation 15 would hold for both the two-parameter and three-parameter fits.

The magnitude of the interaction-length resistance/resistivity expresses that in the flux-flow state when all the defects are in motion, the effective resistivity of the superconductor is still many orders of magnitude less than the normal resistivity of $Nb_3Sn$ above $T_c$.

The Ohmic linearity in field as $B \to 0$ is a feature common to both the interaction resistivity and the flux-flow resistivity. However at fixed reduced field the former increase whereas the latter decreases and the sizes of these two parameters differ for this $Nb_3Sn$ by *seven orders of magnitude*.

It is hardly surprising that these parameters differ so starkly. The flux-flow resistivity describes the dissipation caused by the bulk motion of a perfect fluxon lattice through a defect-free superconductor. The interaction resistivity describes the motion of defects through an otherwise stationary fluxon lattice.

## 7. Conclusion and final comments

In conclusion we point out a very disconcerting feature of these data when compared with other data in the literature. In general, measurements to determine the flux-flow resistivity are not made on wholly defect-free systems. Since these systems have non-zero values for the critical current, the FLL must be distorted and defects in the FLL must be present. Since defect motion (of the interaction type) will occur before bulk flux flow it is clear that these measurements will at best characterise a resistivity which is a combination of the flux-flow resistivity and the interaction resistivity. This obviously undermines any comparison between these measurements and theoretical calculations of the flux-flow resistivity.

This paper has presented data of interest in its own right for the design of high-field superconducting systems. A model has been outlined and experimental data detailed which suggest that in high-current-density materials, above the critical current, it is the motion of defects within the FLL that leads to voltage generation. The universality of the three free parameters used to describe this motion has been measured experimentally and interpreted.

## References


Baixeras J and Fournet G 1967 *J. Phys. Chem. Solids* **28** 1541

Bardeen J and Stephen M J 1965 *Phys. Rev.* **140** A1197

Essman U and Trauble H 1967 *Phys. Lett.* **24A** 526

Evetts J E and Plummer C J G 1985 *Proc. Int. Symp. Flux Pinning and Electromagnetic Properties in Superconductors (Fukuoka, Japan) 1985* ed. T Matsushita, K Yamafuji and F Irie (Fukuoka: Matsukuma) p 146

Fietz D H and Webb W W 1969 *Phys. Rev.* **178** 657

Flukiger R 1984 *KFK Karlsruhe Internal Report*

Foner S and McNiff E J Jr 1981 *Solid State Commun.* **39** 959

Gorkov L P and Kopnin N P 1973 *JETP Lett.* **37** 183

Habbal F and Joiner W C H 1977 *J. Low Temp. Phys.* **28** 83

Hampshire D P and Jones H 1986 *IEEE Trans. Magn.* **MT-9** 531

—— 1987 *J. Phys. E: Sci. Instrum.* **20** 516

Jones R G, Rhoderick E H and Rose-Innes A C 1967 *Phys. Lett.* **24A** 318

Kupfer H and Meier-Hirmer R 1985 *Proc. Int. Symp. Flux Pinning and Electromagnetic Properties in Superconductors (Fukuoka, Japan) 1985* ed. T Matsushita, K Yamafuji and F Irie (Fukuoka: Matsukuma) p 50

Plummer C J G and Evetts J E 1986 *ASC, Baltimore, Report* MF-6 to be published

Singh O, Curzon A E and Koch C C 1976 *J. Phys. D: Appl. Phys.* **9** 611

Smathers D B, Marken K R, Lee P J and Larbalestier D C 1984 *IEEE Trans. Magn.* **M-21** 1133

Tinkham M 1964 *Phys. Rev. Lett.* **13** 804

Walter C R 1974 *Brookhaven Laboratory Informal Report* BNL 18928 (AADD 74-2) 30–1

Warnes W H and Larbalestier D C 1986 *Cryogenics* **26** 632